Material assignment for proton range prediction in Monte Carlo patient simulations using stopping-power datasets

Fibiani-Permatasari, F.; Eulitz, J.; Richter, C.; Wohlfahrt, P.; Lühr, A.; (Editors)

Originally published:

September 2020

Physics in Medicine and Biology 65(2020)18, 185004

DOI: https://doi.org/10.1088/1361-6560/ab9702

Physics in Medicine & Biology

Material assignment for proton range prediction in Monte Carlo patient simulations using stopping-power datasets

To cite this article before publication: Felicia Fibiani Permatasari *et al* 2020 *Phys. Med. Biol.* in press https://doi.org/10.1088/1361-6560/ab9702

IOP Publishing Physics in Medicine and Biology
Journal **PMB** (XXXX) XXXXXX https://doi.org/XXXX/XXXX

Material assignment for proton range prediction in Monte Carlo patient simulations using stopping-power datasets

Felicia Fibiani Permatasari [1,2], Jan Eulitz [2-4], Christian Richter [2-5], Patrick Wohlfahrt [2,4,a,b,†] and Armin Lühr [2,4-5,c,†]

[1] Department of Radiation Oncology, Universitätsmedizin Mannheim, Medical Faculty Mannheim, University of Heidelberg, Mannheim, Germany
[2] OncoRay – National Center for Radiation Research in Oncology, Faculty of Medicine and University Hospital Carl Gustav Carus, Technische Universität Dresden, Helmholtz-Zentrum Dresden-Rossendorf, Dresden, Germany
[3] Department of Radiotherapy and Radiation Oncology, Faculty of Medicine and University Hospital Carl Gustav Carus, Technische Universität Dresden, Dresden, Germany
[4] Helmholtz-Zentrum Dresden-Rossendorf, Institute of Radiooncology – OncoRay, Dresden, Germany
[5] German Cancer Consortium (DKTK), Partner Site Dresden, and German Cancer Research Center (DKFZ), Heidelberg, Germany.

E-mail: felicia.permatasari@uniklinikum-dresden.de

[a] Now with: Massachusetts General Hospital and Harvard Medical School, Department of Radiation Oncology, Boston, MA, USA
[b] ORCID iD: 0000-0002-2121-0934
[c] ORCID iD: 0000-0002-9450-6859
[†] Both authors contributed equally to this work

Abstract

Motivation and objective: For each institute, the selection and calibration of the most suitable approach to assign material properties for Monte Carlo (MC) patient simulation in proton therapy is a major challenge. Current conventional approaches based on computed tomography (CT) depend on CT acquisition and reconstruction settings. This study proposes a material assignment approach, referred to as MATA (**MAT**erial **A**ssignment), which is independent of CT scanner properties and, therefore, universally applicable by any institute.
Materials and methods: The MATA approach assigns material properties to the physical quantity stopping-power ratio (SPR) using a set of 40 material compositions specified for human tissues and linearly determined mass density. The application of clinically available CT-number-to-SPR conversion avoids the need for any further calibration. The MATA approach was validated with homogeneous and heterogeneous SPR datasets by assessing the SPR accuracy after material assignment obtained either based on dose scoring or determination of water-equivalent thickness. Finally, MATA was applied on patient datasets to evaluate dose differences induced by different approaches for material assignment and SPR prediction.
Results: The deviation between the SPR after material assignment and the input SPR was close to zero in homogeneous datasets and below 0.002 (0.2% relative to water) in heterogeneous datasets, which was

IOP Publishing Physics in Medicine and Biology
Journal **PMB** (XXXX) XXXXXX https://doi.org/XXXX/XXXX

within the systematic uncertainty in SPR estimation. The comparison of different material assignment approaches revealed relevant differences in dose distribution and SPR. The comparison between two SPR prediction approaches, a standard look-up table and direct SPR determination from dual-energy CT, resulted in patient-specific mean proton range shifts between 1.3 mm and 4.8 mm.
Conclusion: MATA eliminates the need for institution-specific adaptations of the material assignment. It allows for using any SPR dataset and thus facilitates the implementation of more accurate SPR prediction approaches. Hence, MATA provides a universal solution for patient modeling in MC-based proton treatment planning.

Keywords: Monte Carlo simulation, TOPAS, stopping-power ratio, dual-energy CT, proton radiotherapy

1. Introduction

Proton therapy is an important modality in radiation oncology as its unique physical properties allow to reduce dose to healthy tissue while achieving a highly conformal coverage of the targeted tumor region (Baumann *et al.*, 2016; Bortfeld and Loeffler, 2017). However, range uncertainty currently restricts the full exploitation of the physical capabilities of proton beams for an optimal sparing of healthy tissue. Proton treatment planning in particular is affected by range uncertainties in the order of 3-5% arising from the modeling of the patient geometry using computed tomography (CT) and the dose calculation algorithm (Paganetti, 2012). The CT-related uncertainty is mainly attributed from the prediction of proton range in the patient based on the tissue-specific stopping-power ratio (SPR), which describes the proton stopping power in a material relative to the one in water. Almost all clinical proton centers routinely acquire single-energy CT (SECT) scans and use an institute-specific conversion for SPR prediction (Taasti *et al.*, 2018). To model the energy loss of protons in each CT voxel, common treatment planning systems (TPS) convert the respective CT number (CTN) to SPR or mass density (associated with a material assignment based on mass density) using a piecewise linear heuristic conversion, which is also referred to as Hounsfield look-up table (HLUT) (Schneider *et al.*, 1996).

Monte Carlo (MC) simulations are considered as current gold standard for proton dose calculation (Guatelli and Incerti, 2017). Due to a continuous increase in computational performance, they are nowadays more widely used clinically. In addition to proton treatment planning, they also play an essential role in beam model and plan validation, quality assurance as well as modeling of relative biological effectiveness (RBE) and normal tissue complication probability (NTCP). In contrast to analytical algorithms, MC simulations require an accurate assignment of material properties, such as mass density

and elemental composition, to ensure a precise modeling of physical interactions (Jiang *et al.*, 2007; Wu *et al.*, 2015; España and Paganetti, 2010; Paganetti *et al.*, 2008). Since the material assignment is an essential requirement to achieve the intended accuracy and robustness of MC dose calculation in patients, various approaches have been proposed to assign material properties based on CT (du Plessis *et al.*, 1998; Schneider *et al.*, 2000; Vanderstraeten *et al.*, 2007). Common MC frameworks use a CTN-based material assignment, where the mass density is linearly correlated with CT numbers and the elemental composition is specified according to pre-defined CTN intervals for a limited number of materials. Although these approaches have been demonstrated to be effective, the selection of the most suitable approach and its calibration dedicated to the CT acquisition and reconstruction settings in each institution is a cumbersome and time-consuming process, which has to be performed by each institute individually. This is often an underestimated challenge, in particular for new proton therapy centers with limited resources and expertise.

The CT-based SPR prediction (considering institute-specific CT scan and reconstruction settings) is in general independent from the dose calculation algorithm itself. The same SPR should be derived from the same input CT number to ensure a meaningful assessment of differences in dose calculation between analytical and MC models. Currently, this requires non-trivial calibration steps to synchronize the SPR prediction between the two dose calculation algorithms (Paganetti, 2012; Paganetti *et al.*, 2008). The time-intensive and institution-specific adaptation process can easily introduce an additional source of uncertainty and lead to preventable intra- and inter-center variation due to the lack of a standardized calibration procedure.

In this manuscript, we introduce an institute-independent approach for material assignment in MC patient simulations, referred to as MATA (**MAT**erial **A**ssignment), which directly assigns material properties to SPR. The use of the physical quantity SPR makes MATA independent from CT acquisition and reconstruction settings and, hence, no additional institute-specific adaptation of the material assignment is required for MC algorithms. Furthermore, the SPR-based MATA approach allows MC simulations to utilize any SPR dataset derived from, e.g., SECT, dual-energy CT (DECT), multi-energy CT (MECT) or even proton/helium CT without additional effort. Thus, MC dose calculation could directly benefit from the reduction of the CT-related range uncertainty achievable by patient-specific SPR prediction from DECT (Wohlfahrt and Richter, 2020) as well as directly utilize the same SPR information as used by other dose calculation algorithms for comparative studies.

The physical principles and performance of the MATA approach are described in the following. Its clinical applicability and reliability in terms of SPR accuracy, with respect to the imported reference SPR

dataset, were validated in homogeneous and hetereogenous artificial SPR datasets, an anthropomorphic head phantom as well as three patient cases. In addition to the proof-of-concept evaluation, the impact of MATA on clinical MC dose calculation was studied for patients with different tumor locations (brain, lung and prostate) by comparing several SPR prediction methods based on SECT and DECT as well as different material assignment approaches.

2. Materials and methods

2.1 Basic definitions and notation

The ion stopping power of a material,

$$-\frac{\mathrm{d}E}{\mathrm{d}x} = K \cdot \rho \cdot \Omega(\omega_i) \cdot L(I), \tag{1}$$

can be described with the Bethe equation (Bethe, 1930) as product of a beam-dependent factor, K, and three material-dependent factors, namely, mass density, ρ, material weighted factor, $\Omega(\omega_i)$, and stopping number, $L(I)$.

The beam-dependent factor, K, is given by

$$K = 2\pi N_\mathrm{a} {r_\mathrm{e}}^2 m_\mathrm{e} c^2 \frac{z^2}{\beta^2}, \tag{2}$$

where N_a is the Avogadro number, c is the speed of light, m_e and r_e are the electron mass and classical electron radius, z is the charge of the incident particle ($z = 1$ for proton), and β is the ion velocity divided by c. According to the Bragg-Kleeman additivity rule (Bragg and Kleeman, 1905), the material weighted factor of a mixture or compound is a weighted sum of each single element *i*:

$$\Omega(\omega_i) = \sum_i \omega_i \frac{Z_i}{A_i}, \tag{3}$$

with ω, Z, and A as weighted ratio, atomic number and mass number of the element, respectively. Ignoring higher order correction terms, the stopping number, $L(I)$, which depends on the material-specific mean excitation energy, *I*, is given as

$$L(I) \approx \ln\left(\frac{2m_\mathrm{e}c^2\beta^2}{I(1-\beta^2)}\right) - \beta^2. \tag{4}$$

The ion medium-to-water SPR can be expressed as the product,

$$\mathrm{SPR} = \hat{\rho} \cdot \hat{\Omega}(\omega_i) \cdot \hat{L}(I), \tag{5}$$

where the factors denoted with hat, $\hat{\rho}$, $\hat{\Omega}(\omega_i)$, and $\hat{L}(I)$, represent each of the three factors in medium divided by the corresponding factor in water.

Table 1. MATA for the import of any externally derived stopping-power ratio (SPR) dataset in Monte Carlo simulation. Material assignment for various anatomical regions, i.e. brain, pelvis, and other (head and neck, thorax and abdomen) regions (different tissue compositions for materials 13-18) based on tabulated human tissues (Woodard and White, 1986; White *et al.*, 1989). *I*-value and MATA factor, $F_{\text{MATA III}}$, were determined for MATA III.

Material	SPR	*I*-value	$F_{\text{MATA III}}$	Elemental Weight / %											
				H	C	N	O	Na	Mg	P	S	Cl	Ar	K	Ca	Fe
Brain																
1	[-0.024, 0.024]	88.00	1.130	0	0.012	75.527	23.178	0	0	0	0	0	1.283	0	0	0
2	[0.025, 0.074]	85.05	1.102	2.06	2.110	61.041	33.522	0.04	0	0.04	0.06	0.06	1.026	0.04	0	0
3	[0.075, 0.124]	82.31	1.076	4.12	4.207	46.556	43.867	0.08	0	0.08	0.12	0.12	0.770	0.08	0	0
4	[0.125, 0.174]	79.77	1.051	6.18	6.305	32.071	54.211	0.12	0	0.12	0.18	0.18	0.513	0.12	0	0
5	[0.175, 0.224]	77.39	1.027	8.24	8.402	17.585	64.556	0.16	0	0.16	0.24	0.24	0.257	0.16	0	0
6	[0.225, 0.699]	75.17	1.004	10.3	10.5	3.1	74.9	0.2	0	0.2	0.3	0.3	0	0.2	0	0
7	[0.700, 0.749]	72.59	0.998	10.56	22.02	2.52	63.88	0.18	0	0.16	0.26	0.26	0	0.16	0	0
8	[0.750, 0.799]	70.11	0.991	10.82	33.54	1.94	52.86	0.16	0	0.12	0.22	0.22	0	0.12	0	0
9	[0.800, 0.849]	67.73	0.984	11.08	45.06	1.36	41.84	0.14	0	0.08	0.18	0.18	0	0.08	0	0
10	[0.850, 0.899]	65.44	0.978	11.34	56.58	0.78	30.82	0.12	0	0.04	0.14	0.14	0	0.04	0	0
11	[0.900, 0.924]	63.24	0.972	11.6	68.1	0.2	19.8	0.1	0	0	0.1	0.1	0	0	0	0
12	[0.925, 0.949]	64.78	0.976	11.4	59.8	0.7	27.8	0.1	0	0	0.1	0.1	0	0	0	0
13	[0.950, 0.974]	66.32	0.981	11.2	51.7	1.3	35.5	0.1	0	0	0.1	0.1	0	0	0	0
14	[0.975, 0.999]	70.89	0.989	11.15	25.85	0.65	61.75	0.3	0	0	0.05	0.25	0	0	0	0
15	[1.000, 1.014]	75.79	0.998	11.1	0	0	88	0.5	0	0	0	0.4	0	0	0	0
16	[1.015, 1.024]	74.87	0.999	10.875	7.225	1.075	79.7	0.35	0	0.175	0.1	0.35	0	0.15	0	0
17	[1.025, 1.039]	73.95	0.999	10.65	14.45	2.15	71.4	0.2	0	0.35	0.2	0.3	0	0.3	0	0
18	[1.040, 1.059]	74.62	1.004	10.2	14.3	3.4	71	0.1	0	0.2	0.3	0.1	0	0.4	0	0
19	[1.060, 1.074]	76.30	1.010	9.9	12.1	2.8	72.7	0.3	0	1.2	0.6	0.2	0	0.2	0	0
20	[1.075, 1.089]	78.02	1.016	9.6	9.9	2.2	74.4	0.5	0	2.2	0.9	0.3	0	0	0	0
21	[1.090, 1.129]	79.36	1.021	9.29	10.18	2.3	72.855	0.48	0.01	2.605	0.87	0.285	0	0	1.125	0
22	[1.130, 1.169]	80.74	1.027	8.98	10.46	2.4	71.31	0.46	0.02	3.01	0.84	0.27	0	0	2.25	0
23	[1.170, 1.199]	82.14	1.032	8.67	10.74	2.5	69.765	0.44	0.03	3.415	0.81	0.255	0	0	3.375	0
24	[1.200, 1.229]	83.58	1.037	8.36	11.02	2.6	68.22	0.42	0.04	3.82	0.78	0.24	0	0	4.5	0
25	[1.230, 1.259]	85.05	1.043	8.05	11.3	2.7	66.675	0.4	0.05	4.225	0.75	0.225	0	0	5.625	0
26	[1.260, 1.294]	86.56	1.048	7.74	11.58	2.8	65.13	0.38	0.06	4.63	0.72	0.21	0	0	6.75	0
27	[1.295, 1.329]	88.10	1.054	7.43	11.86	2.9	63.585	0.36	0.07	5.035	0.69	0.195	0	0	7.875	0
28	[1.330, 1.359]	89.68	1.059	7.12	12.14	3	62.04	0.34	0.08	5.44	0.66	0.18	0	0	9	0
29	[1.360, 1.389]	91.30	1.065	6.81	12.42	3.1	60.495	0.32	0.09	5.845	0.63	0.165	0	0	10.125	0
30	[1.390, 1.419]	92.96	1.071	6.5	12.7	3.2	58.95	0.3	0.1	6.25	0.6	0.15	0	0	11.25	0
31	[1.420, 1.449]	94.66	1.076	6.19	12.98	3.3	57.405	0.28	0.11	6.655	0.57	0.135	0	0	12.375	0
32	[1.450, 1.479]	96.40	1.082	5.88	13.26	3.4	55.86	0.26	0.12	7.06	0.54	0.12	0	0	13.5	0
33	[1.480, 1.509]	98.18	1.088	5.57	13.54	3.5	54.315	0.24	0.13	7.465	0.51	0.105	0	0	14.625	0
34	[1.510, 1.539]	100.01	1.094	5.26	13.82	3.6	52.77	0.22	0.14	7.87	0.48	0.09	0	0	15.75	0
35	[1.540, 1.569]	101.88	1.100	4.95	14.1	3.7	51.225	0.2	0.15	8.275	0.45	0.075	0	0	16.875	0
36	[1.570, 1.594]	103.80	1.106	4.64	14.38	3.8	49.68	0.18	0.16	8.68	0.42	0.06	0	0	18	0
37	[1.595, 1.624]	105.77	1.112	4.33	14.66	3.9	48.135	0.16	0.17	9.085	0.39	0.045	0	0	19.125	0
38	[1.625, 1.649]	107.78	1.119	4.02	14.94	4	46.59	0.14	0.18	9.49	0.36	0.03	0	0	20.25	0
39	[1.650, 1.679]	109.85	1.125	3.71	15.22	4.1	45.045	0.12	0.19	9.895	0.33	0.015	0	0	21.375	0
40	[1.680, 4.071]	111.97	1.131	3.4	15.5	4.2	43.5	0.1	0.2	10.3	0.3	0	0	0	22.5	0
Others (Head and Neck, Thorax, Abdomen)																
13	[0.950, 0.974]	66.32	0.981	11.2	51.7	1.3	35.5	0.1	0	0	0.1	0.1	0	0	0	0
14	[0.975, 0.994]	67.89	0.985	11	44.22	1.72	42.6	0.1	0	0.04	0.14	0.1	0	0.08	0	0
15	[0.995, 1.009]	69.51	0.990	10.8	36.74	2.14	49.7	0.1	0	0.08	0.18	0.1	0	0.16	0	0
16	[1.010, 1.019]	71.16	0.995	10.6	29.26	2.56	56.8	0.1	0	0.12	0.22	0.1	0	0.24	0	0
17	[1.020, 1.039]	72.87	0.999	10.4	21.78	2.98	63.9	0.1	0	0.16	0.26	0.1	0	0.32	0	0
18	[1.040, 1.059]	74.62	1.004	10.2	14.3	3.4	71	0.1	0	0.2	0.3	0.1	0	0.4	0	0
Pelvis																
13	[0.950, 0.974]	66.32	0.981	11.2	51.7	1.3	35.5	0.1	0	0	0.1	0.1	0	0	0	0
14	[0.975, 0.994]	65.10	0.977	11.35	58.05	1	29.3	0.1	0	0	0.1	0.1	0	0	0	0
15	[0.995, 1.009]	63.90	0.974	11.5	64.4	0.7	23.1	0.1	0	0	0.1	0.1	0	0	0	0
16	[1.010, 1.019]	66.43	0.983	11	52.9	2.1	33.5	0.1	0	0.1	0.1	0.1	0	0.1	0	0
17	[1.020, 1.039]	69.18	0.992	10.5	41.4	3.4	43.9	0	0	0.1	0.2	0.2	0	0.2	0	0.1
18	[1.040, 1.059]	74.62	1.004	10.2	14.3	3.4	71	0.1	0	0.2	0.3	0.1	0	0.4	0	0

2.2 MATA as universal material assignment

The purpose of the MATA approach is a direct assignment of materials based on the physical quantity SPR instead of the scanner-dependent CT number. This allows for an import of SPR datasets, that have been externally generated, e.g., by applying a CTN-to-SPR conversion with institutional HLUT on SECT or an advanced DECT-based SPR prediction method. Table 1 summarizes the 40 materials used in this study, which were specified based on the tabulated human tissues gathered in the International Commission on Radiation Units and Measurements (ICRU) report 44 (Woodard and White, 1986; White *et al.*, 1989). Since various anatomical regions contain different tissue types, in particular soft tissues, the elemental compositions of materials 13-18 were selected according to their occurrence in three different treatment regions divided in (1) brain, (2) pelvis, and (3) others (head and neck, thorax and abdomen). The composition of cerebrospinal fluid and brain tissue (grey and white matter) are included in the brain region, while the compositions of yellow and red marrow are considered in the pelvic region. In other regions, various combinations of adipose and muscle are used. This separation ensures that proper tissues are assigned to each specific region and thus reduces incorrect tissue mappings, e.g. brain tissue should not occur in the pelvis. MATA assigns the respective material properties according to pre-defined SPR intervals, while the mass density is determined as a function of input SPR (subscript input):

$$\rho = F_{\mathrm{MATA}} \cdot \mathrm{SPR}_{\mathrm{input}}, \tag{6}$$

where the MATA factor, F_{MATA}, maintains the input SPR after material assignment,

$$\mathrm{SPR} = \frac{\rho}{\rho_{\mathrm{w}}} \cdot \hat{\Omega}(\omega_i) \cdot \hat{L}(I) \equiv \mathrm{SPR}_{\mathrm{input}}, \tag{7}$$

with ρ_{w} as the density of water. The MATA factor was obtained by three different approaches denoted as MATA I, II, and III.

MATA I

Assigning the *I*-value of each material to the one of water, the MATA factor is simplified as

$$F_{\mathrm{MATA\,I}} = \rho_{\mathrm{w}} \cdot \left[\hat{\Omega}(\omega_i)\right]^{-1}. \tag{8}$$

MATA II

Estimating the material-specific *I*-values using Bragg-Kleeman's additivity rule (Bragg and Kleeman, 1905),

$$I = \exp\left[\frac{\sum_i \omega_i \frac{Z_i}{A_i} \ln I_i}{\sum_i \omega_i \frac{Z_i}{A_i}}\right], \tag{9}$$

with elemental *I*-values from ICRU report 37 (Berger *et al.*, 1984), the MATA factor is calculated as

$$F_{\text{MATA II}} = \rho_{\text{w}} \cdot \left[\widehat{\Omega}(\omega_{\text{i}}) \cdot \hat{L}(I)\right]^{-1}. \quad (10)$$

MATA III

Considering the stopping-power calculation within MC simulation, the MATA factor is determined as

$$F_{\text{MATA III}} = S^{-1}\left(\frac{\text{d}E}{\text{d}x}\right)_{\text{w}}, \quad (11)$$

where $\left(\frac{\text{d}E}{\text{d}x}\right)_{\text{w}}$ is the energy loss in water and S is the mass stopping power of a material given by

$$S = K \cdot \Omega(\omega_i) \cdot L(I)\,. \quad (12)$$

2.3 Implementation of MATA in a Monte Carlo simulation platform

In this work, the MC simulation platform Tool for Particle Simulation (TOPAS) 3.1.p3 (Perl *et al.*, 2012) was exemplarily chosen to realize the methodological concept of MATA. In addition to material properties, Table 1 contains the material-specific *I*-value obtained by Eq. (9) and the respective MATA factor for MATA III according to Eq. (11) using $\left(\frac{\text{d}E}{\text{d}x}\right)_{\text{w, 100 MeV}} = 7.25901\ \text{MeV/cm}$ for implementation of MATA in TOPAS. The *I*-value in TOPAS was overwritten accordingly, i.e. with the *I*-value of water ($I_{\text{w}} = 78$ eV) for MATA I or the calculated *I*-value for the other MATA implementations, respectively.

2.4 Validation of MATA approach

Since MATA is based on a pre-defined SPR dataset, an accurate SPR import and processing needs to be ensured in MC simulations. Hence, the MATA approach was solely validated by assessing the SPR accuracy after material assignment, because the mapping of mass density and elemental composition is ensured by the adequate selection of reference tabulated human tissues from the ICRU report 44 (Woodard and White, 1986; White *et al.*, 1989), which is the current gold standard. The SPR accuracy was evaluated by calculating the SPR difference between the reference SPR and the SPR derived after material assignment. The relative SPR difference was reported with respect to the SPR of water ($\text{SPR}_{\text{w}} = 1$). Figure 1 illustrates the SPR validation scheme of the MATA implementation in TOPAS consisting of a feasibility study (Figure 1A) and an accuracy assessment (Figure 1B). Two approaches for SPR estimation were applied to obtain the SPR after material assignment: water-equivalent thickness (WET) calculation in the feasibility study and a dose scoring method in the accuracy assessment. As the commonly used WET calculation method is limited to homogeneous geometries, the dose scoring method is applied instead to

evaluate MATA in heterogeneous geometries, e.g. anthropomorphic phantoms. A direct comparison of both SPR estimation tools in homogeneous geometries was performed to investigate systematic differences.

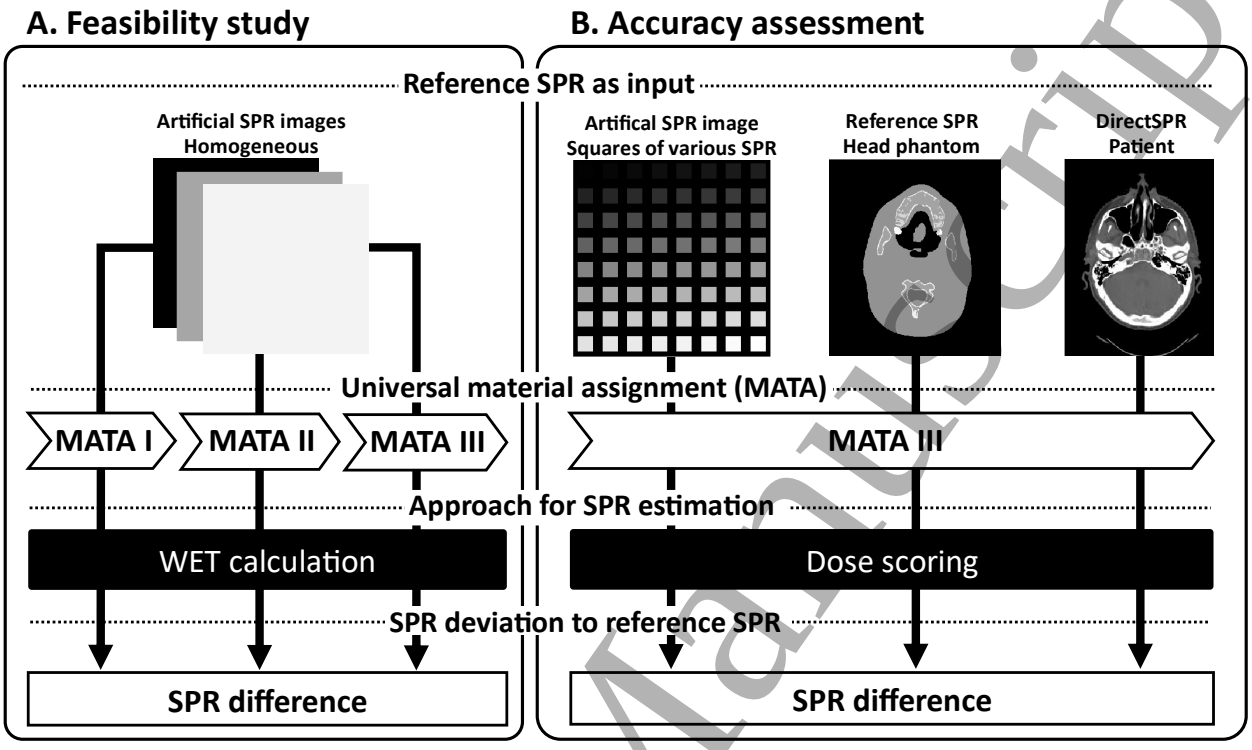

Figure 1. Flowchart for (A) the feasibility study of MATA approaches (I, II, and III) and (B) the accuracy assessment of MATA III. Validation was performed by assessing the stopping-power ratio (SPR) difference between the reference SPR and the SPR after material assignment estimated with water-equivalent thickness (WET) calculation or dose scoring.

2.4.1 Feasibility study

To demonstrate the applicability of the MATA approach (MATA I to III), a homogeneous artificial SPR dataset with an image size of 50×50 cm^2 and thickness of 1 cm was generated for each of the 40 assigned materials (Table 1). All image voxels were set to the median SPR of the respective SPR interval of a material (Figure 1A).

The SPR for each image after material assignment was obtained by WET calculation based on a range estimation in water (Zhang and Newhauser, 2009; Zhang *et al.*, 2010),

$$\mathrm{SPR} = \frac{\mathrm{d}R}{t} = \frac{R_0 - R}{t}, \tag{13}$$

where R and R_0 are the ranges of a proton beam in water with and without a homogeneous SPR image of thickness t positioned in front of the water phantom, respectively, and $\mathrm{d}R$ is the water-equivalent range shift induced by the SPR image. Considering all physical interactions processed in the MC simulation, the depth-dose distribution of a 100 MeV proton pencil beam with more than 10^7 primary protons was calculated in a water phantom (100×100 cm^2 and 30 cm depth) by scoring the dose to water with a depth resolution of 0.1 mm. The proton range at the distal 80% dose was assessed by fitting an analytical model to the Bragg peak curve (Bortfeld, 1997).

2.4.2 Accuracy assessment

The accuracy of MATA was assessed for the most sophisticated method MATA III using inhomogeneous SPR datasets of increased complexity (Figure 1B): (A) an artificial SPR image with 64 homogeneous squares of linearly increasing SPR surrounded by air, (B) six representative axial slices of the reference SPR dataset of an anthropomorphic head phantom (Wohlfahrt *et al.*, 2018a) as well as (C) four representative axial slices of a directly derived SPR dataset from DECT (DirectSPR) of a brain-, prostate- and lung-tumor patient (Wohlfahrt *et al.*, 2017b; Wohlfahrt *et al.*, 2018b). For patient cases, the respective anatomical region was considered for material assignment (Table 1). The brain material assignment was applied to the head phantom.

Following the retroactive conversion of the two dose scorers available in MC simulation, the SPR after material assignment can be estimated with the dose scoring method by

$$\mathrm{SPR} = \frac{\rho}{\rho_\mathrm{w}} \frac{D_\mathrm{m}}{D_\mathrm{w}}, \tag{14}$$

where D_m and D_w are the dose to medium and the dose to water, respectively, both scored in the same MC simulation. In charged particle equilibrium, the dose to medium relative to the dose to water reflects the unrestricted medium-to-tissue collision SPR according to the Bragg-Gray cavity theory (Dogan *et al.*, 2006; Fippel and Nüsslin, 2000; Siebers *et al.*, 2000). Accordingly, for SPR estimation, the two dose scorers need to be used under the condition that both the energy dependence and nuclear interactions are neglected (Paganetti, 2009). Hence, the two dose scorers used within the dose scoring method only considered the dose deposited by primary protons to reduce the influence of nuclear interactions.

Single axial slices were irradiated with a monoenergetic 100 MeV flat proton beam traversing the slice in depth (along the direction of the slice thickness). This resulted in more than 15000 primary protons/voxel. The SPR difference between the reference SPR and SPR estimated with dose scoring was determined for each image voxel.

2.4.3 Comparison between WET calculation and dose scoring for SPR estimation

The dose scoring was compared with the WET calculation method (c.f. section 2.2.1) to estimate systematic differences between the two approaches for SPR estimation. The difference between SPR estimated with WET calculation and dose scoring was calculated for each of the homogeneous artificial SPR images using MATA III and a 100 MeV flat proton beam with 10^7 simulated primary protons.

2.5 Application of MATA approach

After the implementation and thorough evaluation, the application of MATA was demonstrated in a brain-, prostate- and lung-tumor patient treated at the University Proton Therapy Dresden (UPTD). The passively scattered proton treatment plans, consisting of 2-3 treatment fields, were recalculated in MC simulations considering all particle interactions (plan information in Table SA, Supplementary material). The plans were simulated and the dose distributions were calculated using an in-house developed MC simulation framework (Eulitz *et al.*, 2019a). For each simulated patient treatment field, approximately one million protons/cm^2 reached the patient CT geometry resulting in a statistical MC uncertainty of the simulated dose $\leq$ 0.5% in 1×1×2 mm^3 voxels (1×1 mm^2 pixel size with slice thickness of 2 mm) that received more than 2% of the prescribed dose. MC dose distributions were compared for different approaches for material assignment (c.f. section 2.5.1) and SPR prediction (c.f. section 2.5.2). For all patients, voxelwise dose differences and proton range shifts in beam direction were quantified as described in (Wohlfahrt et al., 2017b).

For each patient, a dual-spiral 80/140 kVp DECT scan with a resolution of 1×1×2 mm^3 (1×1 mm^2 pixel size with slice thickness of 2 mm) was acquired at a Siemens single-source CT scanner SOMATOM Definition AS (Wohlfahrt *et al.*, 2017b; Wohlfahrt *et al.*, 2018b). A 79 keV pseudo-monoenergetic CT dataset (Mono79-CTN) was derived from DECT using the module SYNGO.CT DE MONOENERGETIC PLUS of the image post-processing environment SYNGO.VIA (Siemens Healthineers, Forchheim, Germany). This dataset was used for clinical dose calculation at UPTD, because it contains less image noise and provides an improved CTN constancy compared to a 120 kVp SECT scan with the same total CT dose (Wohlfahrt *et al.*, 2017a).

Two SPR datasets were obtained from each DECT scan. First, the institutional HLUT for CTN-to-SPR conversion was applied to the Mono79-CTN dataset to generate the SPR dataset (Mono79-SPR) as used in the clinical TPS (Wohlfahrt *et al.*, 2017b; Wohlfahrt *et al.*, 2018b). Second, a SPR dataset was directly

derived from DECT (DirectSPR) using the RhoSigma approach (Möhler *et al.*, 2016; Wohlfahrt *et al.*, 2017b; Wohlfahrt *et al.*, 2018a).

2.5.1 Comparison of material assignment approaches

The MATA approach based on SPR datasets was compared with two standard material assignment methods based on CTN. The Mono79-CTN dataset was translated into material properties using, first, the TOPAS default material assignment (Figure S and Table SB, Supplementary material) based on (Schneider *et al.*, 2000) as described in (Perl, 2016) and, second, an institutionally adapted material assignment (Figure S and Table SC, Supplementary material). The institute-specific conversion was generated by adapting the TOPAS default material assignment to match the institutional HLUT (Figure S, Supplementary material).

In addition, the Mono79-SPR dataset was translated into material properties using the MATA approach considering the anatomical region-specific materials defined in Table 1. The import of the Mono79-SPR dataset with the MATA approach ensures the effective use of the institutional HLUT (for CTN-to-SPR conversion) within the MC framework and thus serves as reference.

2.5.2 Comparison of SPR prediction methods

Deviations in range and dose within patients in MC simulations originating from the CTN-to-SPR conversion for SPR prediction were assessed using either a HLUT or DirectSPR approach. The MATA method was applied to both Mono79-SPR and DirectSPR datasets derived from the same DECT scan.

3. Results

3.1 Validation of MATA approach

3.1.1 Feasibility study

As shown in Figure 2A, the three MATA implementations maintain the input SPR. The absolute deviation between the reference SPR and the SPR after material assignment estimated with WET calculation is below 0.005 for 40 assigned materials as exemplarily illustrated for the brain-specific material assignment. This corresponds to a relative SPR difference of 0.5% with respect to water.

From MATA I to MATA III, the SPR deviation clearly decreases towards 0. For MATA I, SPR deviations become larger for materials with an *I*-value differing from the one of water. MATA II substantially improves the SPR accuracy with a maximal remaining SPR difference of 0.1% by minimizing the discrepancy in *I*-value assignment. Further refinement with MATA III even removed the residual deviation of 0.1% and thus results in perfect SPR conformity. Hence, results of the following evaluations are exclusively presented based on MATA III.

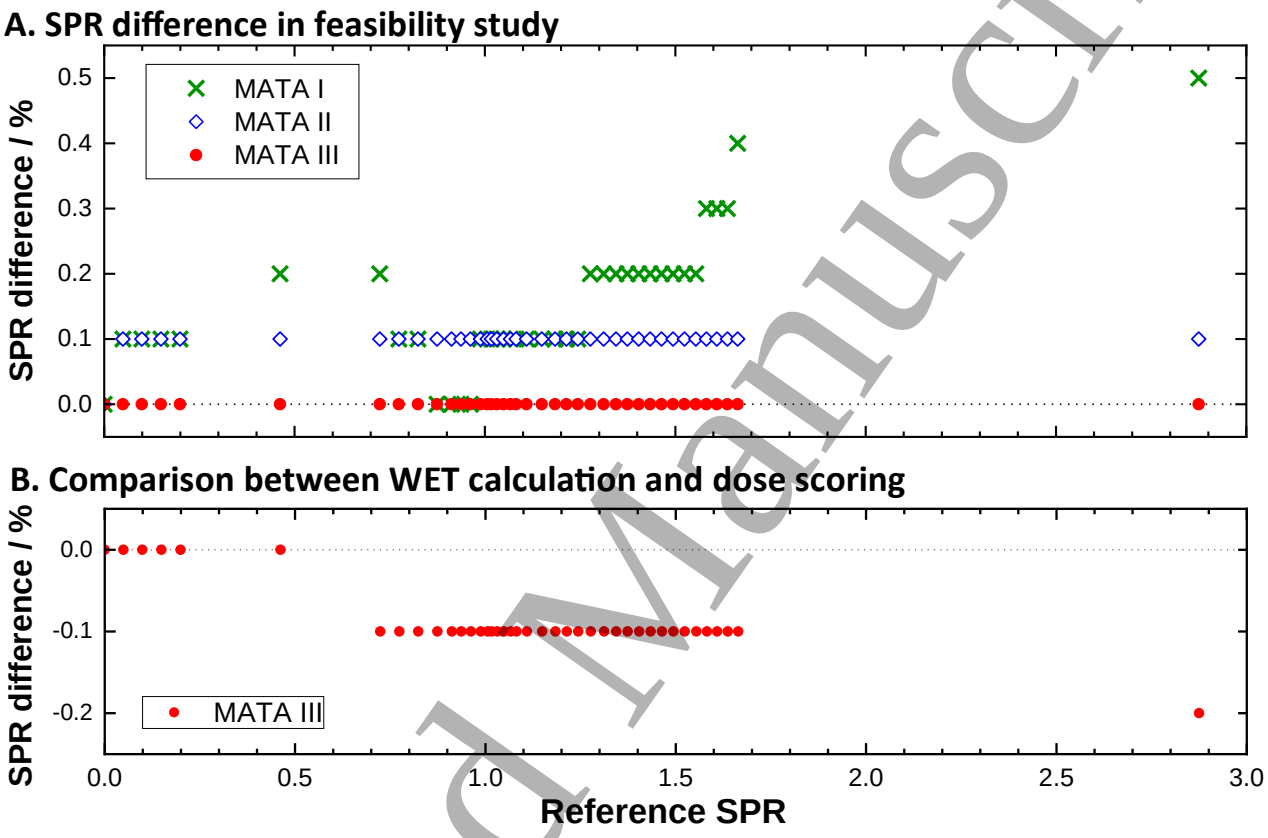

Figure 2. (A) Difference between reference stopping-power ratio (SPR) and SPR estimated in Monte Carlo simulation (with respect to water) using water-equivalent thickness (WET) calculation for the 40 assigned materials (Table 1, brain). (B) SPR difference (with respect to water) of the two approaches for SPR estimation; WET calculation and dose scoring.

3.1.2 Comparison between WET calculation and dose scoring for SPR estimation

Relative SPR differences in MC simulations obtained by WET calculation and dose scoring were within 0.2% with respect to water (Figure 2B). In most cases (SPR > 0.5), a slightly larger SPR was determined by dose scoring. Except for the material with the highest density (SPR = 2.875), the SPR deviation was within 0.1%.

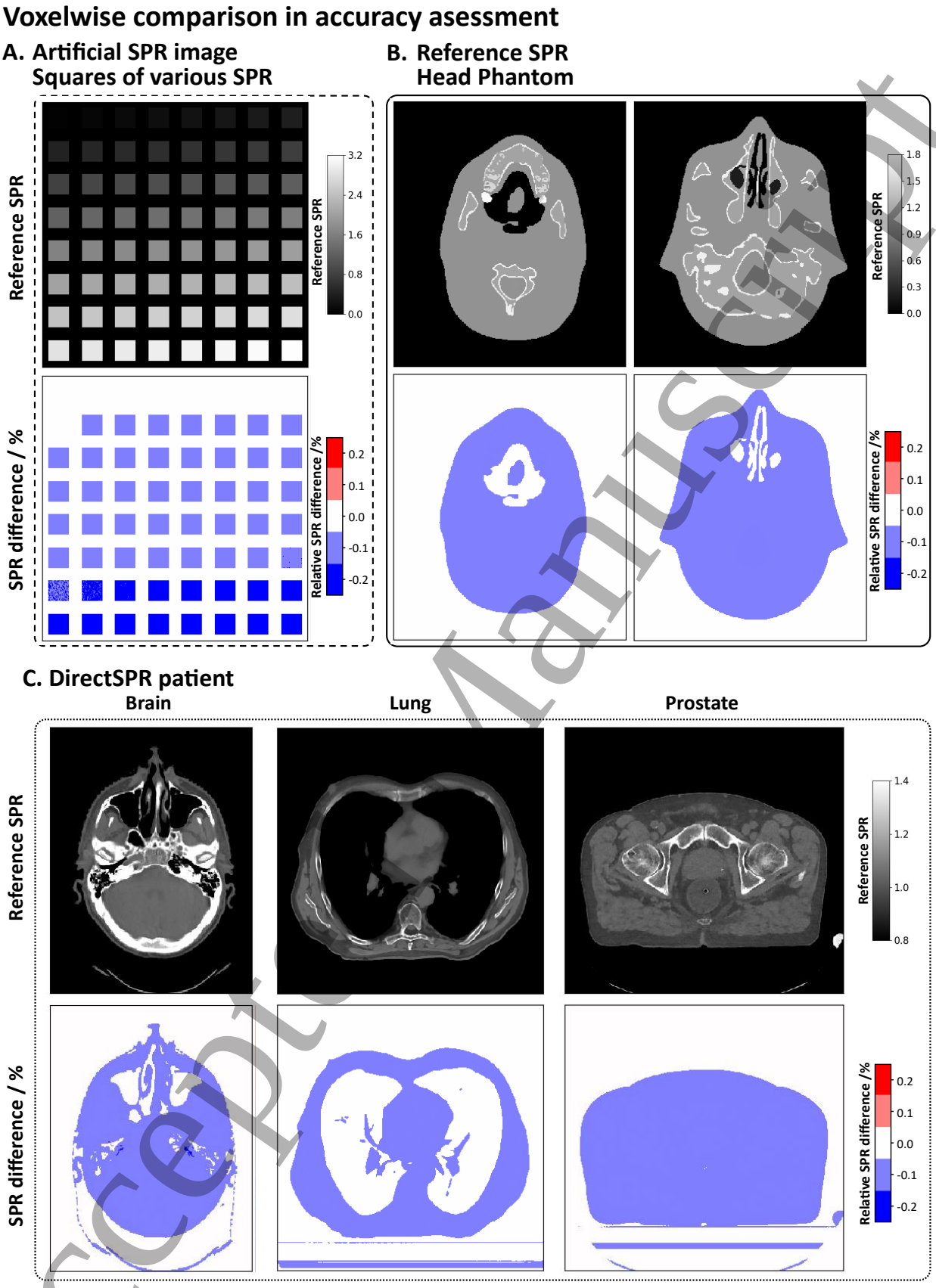

Figure 3. Representative axial slices to compare the reference stopping-power ratio (SPR) and the SPR after material assignment estimated with dose scoring for (A) the artificial SPR image with squares of various SPR, (B) the reference SPR dataset of an anthropomorphic head phantom, and (C) DECT-derived SPR datasets (DirectSPR) of three different patient cases.

3.1.3 Accuracy assessment

For all investigated cases, the SPR datasets obtained with dose scoring in MC simulations corresponded well with the input SPR datasets (Figure 3). The voxelwise SPR difference (with respect to water) was found to be within 0.2%. The evaluation of the artificial SPR dataset with squares of various SPR values (Figure 3A) showed a pattern of SPR-dependent systematic deviations similar to that obtained for the homogeneous SPR images (c.f. section 3.1.2). In the anthropomorphic head phantom (Figure 3B), a maximum SPR difference of 0.1% was found in all soft tissues, teeth and bones ($1.030 \leq SPR \leq 1.763$), as well as no SPR difference for air and sinus cavity ($SPR \leq 0.201$). The same tendency was observed for the more complex and realistic patient datasets (Figure 3C), where SPR values differed up to 0.2% from the input SPR dataset. Only voxels assigned to material 40 showed the maximum SPR difference of 0.2%, while materials 6-39 and 1-5 had a SPR deviation of 0.1% or less, respectively.

3.2 Application of MATA approach

3.2.1 Comparison of material assignment approaches

Different material assignment approaches can lead to noticeable dose differences, especially at the distal dose fall-off, as illustrated in a scheme for an exemplary axial CT slice of a brain-tumor patient (Figure 4, blue arrows). As compared to MATA, the use of the default conversion in TOPAS resulted in relative and absolute mean water-equivalent proton range shifts ± one standard deviation of (0.8 ± 0.7)% and (0.9 ± 0.7) mm for a brain-tumor, (1.7 ± 0.2)% and (4.2 ± 0.5) mm for a prostate-cancer, as well as (1.1 ± 1.4)% and (1.4 ± 1.4) mm for a lung-tumor patient. In contrast to the TOPAS default HLUT, the institutional HLUT systematically predicts larger SPR for CT numbers between -500 HU and 1000 HU covering mixtures of low-density materials with soft tissues, soft tissues as well as low-density bones (Figure S of Supplement). For high-density materials (CT number > 1000 HU), smaller SPRs are estimated by the institutional HLUT.

Adapting the material assignment in TOPAS according to the institutional imaging protocol, the relative and absolute mean water-equivalent proton range shifts ± one standard deviation were reduced to -(0.6 ± 0.6)% and -(0.7 ± 0.7) mm for a brain-tumor, -(0.5 ± 0.1)% and -(1.2 ± 0.3) mm for a prostate-cancer, as well as -(0.2 ± 1.0)% and -(0.2 ± 0.8) mm for a lung-tumor patient. For the institutionally adapted material assignment, the default TOPAS material assignment was adjusted to the institutional HLUT resulting in an SPR difference within 1% for CT numbers below 1500. Larger SPRs are predicted by the institutionally adapted material assignment as compared to the institutional HLUT for high-density materials (CT number > 1500) (Figure S of Supplement).

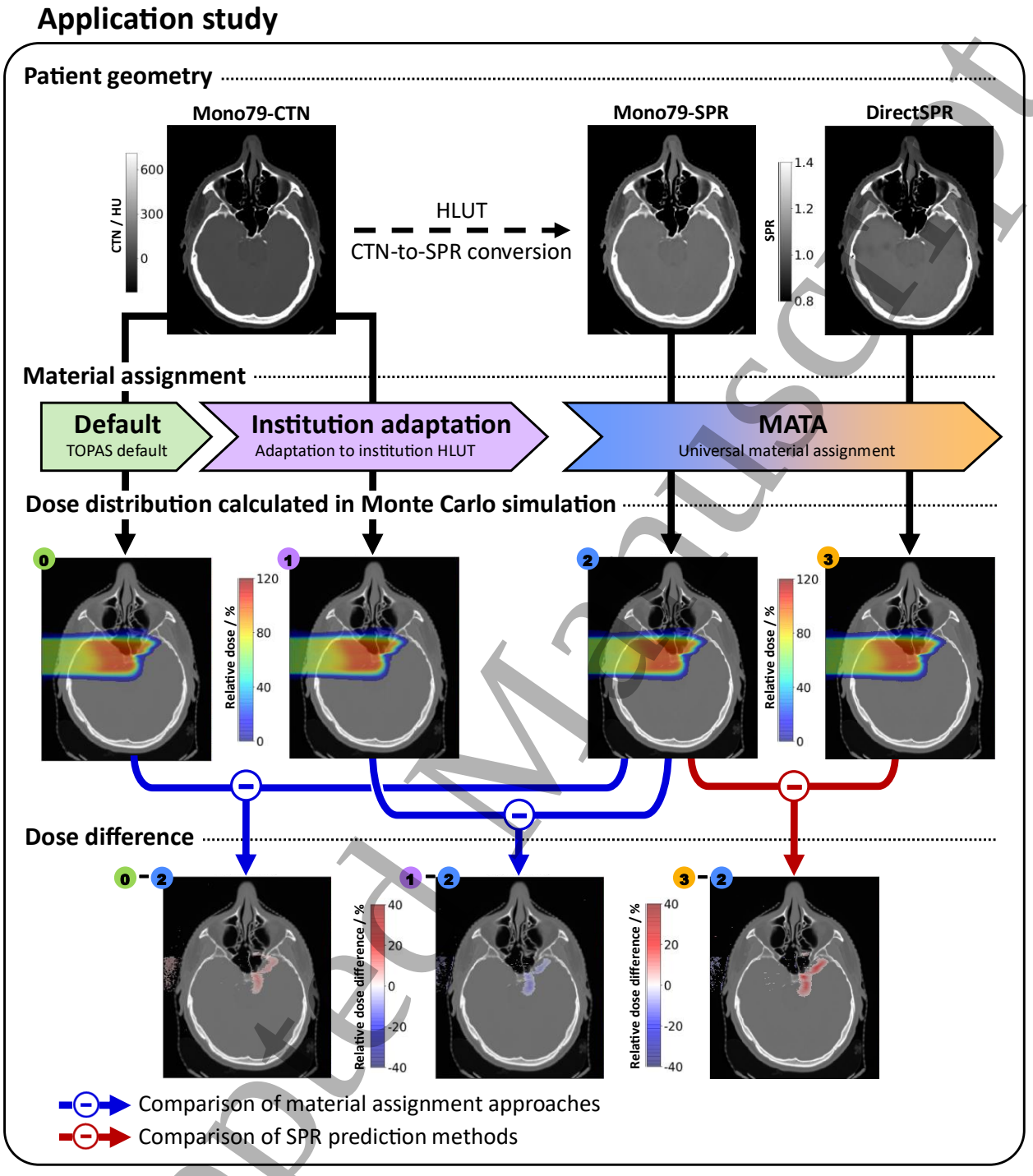

Figure 4. Flow chart for a Monte Carlo simulation of a clinical proton treatment field of a brain-tumor patient, represented by an axial slice of a 79 keV pseudo-monoenergetic CT dataset (Mono79-CTN), a stopping-power ratio (SPR) dataset generated with the clinically applied Hounsfield look-up table (HLUT) based on the state-of-the-art CT-number-to-SPR conversion (Mono79-SPR, used as reference), and a directly derived SPR dataset from DECT (DirectSPR) using the RhoSigma approach. The impact of different material assignment approaches (blue arrows) and different SPR prediction methods (red arrow) on dose calculation is shown for a representative axial slice.

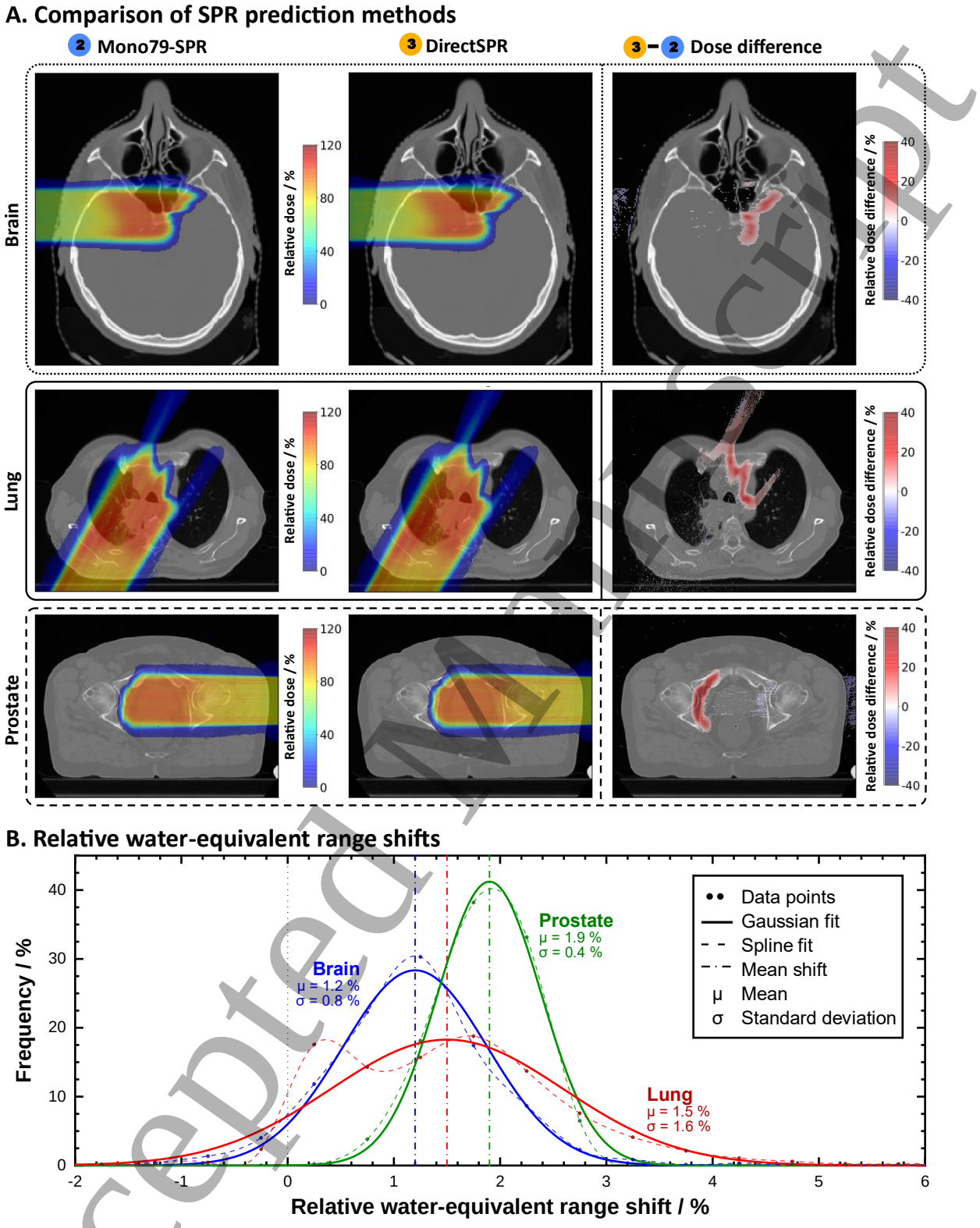

Figure 5. (A) Relative dose distribution of a single treatment field for proton treatment plans of brain-, lung- and prostate-cancer patients obtained by Monte Carlo simulation to compare two different stopping-power ratio (SPR) prediction approaches; the current state-of-the-art method using a Hounsfield look-up table approach (Mono79-SPR) and the patient-specific DECT-derived SPR prediction (DirectSPR). (B) Distribution of relative water-equivalent range shifts calculated for the same patients considering depth-dose profiles of all treatment fields.

3.2.2 Comparison of SPR prediction methods

The MATA approach allows for an accurate import of externally derived SPR datasets in the MC framework. Hence, MATA can be used to compare two SPR prediction approaches within MC simulations which could previously only compared in a clinical TPS: the state-of-the-art SPR prediction method using a HLUT (standard CTN-to-SPR conversion) and the more accurate DirectSPR method (Figure 4, red arrow). For the three different patient cases, Figure 5A illustrates the impact of the two SPR prediction techniques on the dose distribution for an exemplary treatment field. On average, the DirectSPR approach predicts larger proton ranges compared with the institutional HLUT. Based on the evaluation of depth-dose curves in beam direction for all investigated treatment fields, relative and absolute mean water-equivalent proton range shifts ± one standard deviation of (1.2 ± 0.8)% and (1.3 ± 0.9) mm for a brain-tumor, (1.9 ± 0.4)% and (4.8 ± 1.2) mm for a prostate-cancer, as well as (1.5 ± 1.6)% and (1.9 ± 1.6) mm for a lung-tumor patient were determined (Figure 5B). The smallest range shifts were observed in the brain-tumor patient. The lung-tumor patient showed the largest variation in range shifts within a treatment field.

4. Discussion

In this study, a universal method for material assignment (MATA) in MC patient simulations for proton therapy is introduced. By deploying the physical quantity SPR instead of CT numbers, which rely on CT acquisition and reconstruction settings, MATA separates the institute-specific SPR determination from MC dose computation. The comprehensive evaluation showed that MATA is a simple and robust tool for an accurate import of externally generated SPR datasets in a MC framework. With the most sophisticated MATA approach (MATA III), SPR information in each voxel could be fully maintained and applied in MC simulations. Even the simplest option (MATA I), which neglects the material dependence of the *I*-value, led to SPR deviations within 0.5%. The import of SPR datasets – generated either with an HLUT or derived from DirectSPR into an MC environment – was successfully demonstrated. The material properties are assigned based on the current international standard for human tissues. Thus, MATA supports the combination of any SPR prediction technique with MC simulations in proton therapy and, therefore, facilitates further progress in MC-based treatment planning. The feasibility and proper applicability of MATA was also demonstrated for inhomogeneous geometries. The reference SPR of each voxel was reproduced within the systematic uncertainty of the dose scoring method.

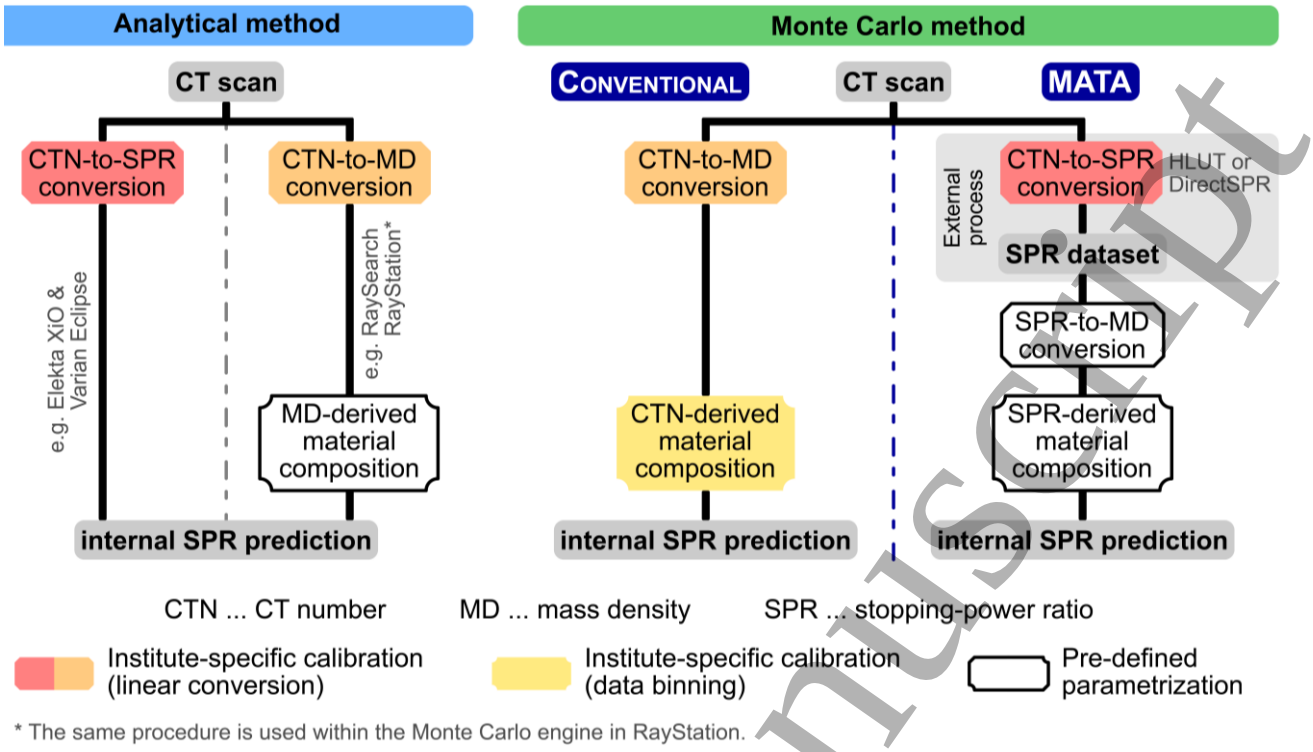

Figure 6. Flowchart describing the procedures for internal stopping-power ratio (SPR) prediction for both analytical and Monte Carlo methods including the comparison between the conventional approach for CT-number-based material assignment and MATA approach for SPR-based material assignment.

One major advantage of the MATA approach is the standardization of material assignment in MC patient simulations using the physical quantity SPR as input. In contrast, the conventional approaches (du Plessis *et al.*, 1998; Schneider *et al.*, 2000; Vanderstraeten *et al.*, 2007) require that each institute performs its own adaptation of the CTN-based material assignment, which is dedicated to their CT scan protocol and institutional HLUT (Figure 6). Typically, this adaptation includes the calibration of both, the mass density and the material composition assignment and is therefore cumbersome and time-consuming. On the other hand, MATA provides a universal material assignment that is independent from the pre-processing method used for SPR dataset generation. By ensuring the use of the same SPR prediction in analytical and MC dose calculation, MATA eliminates the need for individual adaptations of the material assignment as well as the uncertainty and intra- and inter-center variability related to this process. As a general approach, MATA is not restricted to a specific MC tool. Here, the feasibility and potential of MATA for material assignment were successfully demonstrated in TOPAS. The implementation of MATA in other simulation platforms is possible by adopting MATA in the imaging-to-material framework. Thus, MATA facilitates comparability and reproducibility of dose calculations among MC simulations as well as data exchange between several proton therapy facilities.

Another notable benefit of MATA is the straightforward implementation of more accurate SPR prediction approaches in MC simulations. By design, any SPR dataset can be imported in the MC framework, making MATA attractive for direct comparisons between different SPR prediction approaches based on SECT, DECT, MECT or even proton/helium CT. Here, the impact of improved range prediction using the DECT-based DirectSPR approach, previously investigated in a commercial TPS (Wohlfahrt *et al.*, 2017b; Wohlfahrt *et al.*, 2018b; Wohlfahrt *et al.*, 2019), was cross-validated in MC dose calculation for brain-, prostate-, and lung-tumor patients. Relative proton range shifts of clinical relevance (on average about 1-2%) were observed in the MC dose distributions between the heuristic HLUT and the DirectSPR approach. The relative water-equivalent range shifts derived in MC simulations are in good agreement with those assessed for 25 brain-tumor and 25 prostate-cancer patients using an analytical algorithm for dose calculation in a commercial TPS (Wohlfahrt *et al.*, 2017b). Interestingly, slightly different range shifts were obtained for lung-tumor patients (Wohlfahrt *et al.*, 2018b). The deviations may originate from the different handling of multiple Coloumb scattering in severely inhomogeneous anatomical regions between an analytical and MC algorithm (Grassberger *et al.*, 2014). Accordingly, the improved range prediction from patient-specific DirectSPR prediction, which was earlier demonstrated in TPS, has been successfully transferred to MC simulations. Currently ongoing studies that determine the clinical proton RBE and NTCP in patients already profit from the improved range accuracy that is enabled by MATA (Eulitz *et al.*, 2019a; Eulitz *et al.*, 2019b). For these studies, an accurate proton range prediction is crucial to correctly spatially correlate treatment-induced lesions in healthy tissue with dosimetric parameters and areas of increased linear energy transfer at the distal edge of proton treatment fields.

Apart from the conventional material assignment approaches (du Plessis *et al.*, 1998; Schneider *et al.*, 2000; Vanderstraeten *et al.*, 2007), which are widely utilized in SECT, various tissue decomposition techniques based on DECT (Hünemohr *et al.*, 2014; Landry *et al.*, 2013) or MECT (Lalonde and Bouchard, 2016) have been proposed. The extraction of additional information from two or multiple energies with DECT or MECT, such as electron density and effective atomic number, might allow for a more accurate specification of the elemental composition and mass density in MC simulations. So far, the feasibility of these methods for dose calculation was demonstrated on a few patient datasets within retrospective research studies (Almeida *et al.*, 2018; Lalonde *et al.*, 2019). An improved classification of materials should be pursued to further increase the accuracy and precision of MC dose calculation, because proton scattering and nuclear interactions could be modeled more realistically in MC simulations. However, the impact of advanced material decomposition methods on range calculation is expected to be small if a correctly determined SPR can be ensured in the simulation, e.g. through DirectSPR import with

MATA. The ability of each institute to implement these tissue decomposition methods strongly depends on their experience, capability and time availability. Only institutes with DECT capability as well as a thorough understanding of the decomposition approaches could nowadays implement this in MC environments. In contrast, MATA can be easily used by any institute regardless of the CT scanner / modality used in the institute (c.f. MATA user instruction, Supplementary material).

Two approaches for SPR estimation, referred to as WET calculation and dose scoring, have been presented and compared. The WET calculation is equivalent to a proton transmission measurement, typically used for SPR assessment based on homogeneous material slabs. While this approach is considered to be reliable, its application is difficult in heterogeneous patient geometries. Consequently, the dose scoring technique, which is less widely used for SPR estimation in MC simulations, was applied to evaluate the MATA approach in more realistic and complex cases. The comparison of both methods revealed that using dose scoring resulted in a systematic uncertainty in SPR estimation of up to 0.2%, which decreased with decreasing SPR.

The MATA approach relies on some simplifications. First, as MATA assumes an accurate SPR dataset as input, the resolution of the SPR dataset, e.g. three significant fractional digits in the current implementation, as well as the accuracy of the SPR prediction technique limit the overall SPR precision and thus the accuracy of MC simulations. Second, higher-order correction terms of the Bethe equation and the energy dependence of SPR were neglected. The impact on the SPR that is effectively used in the MC simulations is, however, practically negligible as can be concluded from the performed accuracy assessment. Third, to reduce the complexity and minimize the computation time, the material composition is limited to 40 tabulated human tissues in the whole SPR range from -0.024 to 4.071 (Table 1). This might have a small influence, e.g., on interaction cross sections and therefore exact secondary particle production. The potential influence on scattering and energy straggling of protons was studied but had hardly any impact on the simulated dose distributions.

The demands and benefits of future standardization and harmonization in particle therapy have been identified, recommended and proposed in several studies, e.g., for SPR prediction (Taasti *et al.*, 2018; Wohlfahrt and Richter, 2020), image-guided particle therapy (Bolsi *et al.*, 2018), radiobiological experiments (Dosanjh *et al.*, 2018), and treatment planning (Giebeler *et al.*, 2013). Along these lines, MATA supports the standardization in MC-based treatment planning as universal material assignment approach. To foster the intended standardization and harmonization in proton therapy, we recommend that all major MC simulation platforms applied for patient dose calculation implement the functionality to directly perform MC simulations on SPR datasets using the MATA approach.

5. Conclusion

The complexity and influence of CTN-based material assignment for Monte Carlo patient simulations are often underestimated. In this work, an approach for material assignment (MATA) based on the physical quantity SPR was introduced. MATA opens a path to standardize the material assignment for patient modeling in MC simulations and removes the necessity of having multiple dedicated CT-based material assignments. It allows for incorporating any SPR prediction technique and thus enables the implementation of patient-specific DECT-based SPR prediction in MC simulations, which provides an improved range prediction. Thus, MATA facilitates the combination of Monte Carlo as the most accurate dose calculation approach with any SPR prediction technique for proton therapy simulations in a convenient way.

Acknowledgements

The authors are grateful to Dr. Benjamin Lutz for providing support with the perfomed Monte Carlo simulations. This work has been partially supported by StrahlenSchutzSeminar in Thüringen e.V.

References

Almeida I P, Schyns L, Vaniqui A, van der Heyden B, Dedes G, Resch A F, Kamp F, Zindler J D, Parodi K, Landry G and Verhaegen F 2018 Monte Carlo proton dose calculations using a radiotherapy specific dual-energy CT scanner for tissue segmentation and range assessment *Phys. Med. Biol.* **63** 115008

Baumann M, Krause M, Overgaard J, Debus J, Bentzen S M, Daartz J, Richter C, Zips D and Bortfeld T 2016 Radiation oncology in the era of precision medicine *Nature Reviews Cancer* **16** 234

Berger M J, Inokuti M, Anderson H H, Bichsel H, Dennis J A, Powers D, Seltzer S M and Turner J E 1984 ICRU Report 37: Stopping Powers for Electrons and Positrons *International Commission on Radiation Units and Measurements*

Bethe H 1930 Zur Theorie des Durchgangs schneller Korpuskularstrahlen durch Materie *AnP* **397** 325-400

Bolsi A, Peroni M, Amelio D, Dasu A, Stock M, Toma-Dasu I, Nyström P W and Hoffmann A 2018 Practice patterns of image guided particle therapy in Europe: A 2016 survey of the European Particle Therapy Network (EPTN) *Radiother. Oncol.* **128** 4-8

Bortfeld T 1997 An analytical approximation of the Bragg curve for therapeutic proton beams *Med. Phys.* **24** 2024-33

Bortfeld T R and Loeffler J S 2017 Three ways to make proton therapy affordable *Natur* **546**

Bragg W H and Kleeman R 1905 XXXIX. On the α particles of radium, and their loss of range in passing through various atoms and molecules *The London, Edinburgh, and Dublin Philosophical Magazine and Journal of Science* **10** 318-40

Dogan N, Siebers J V and Keall P J 2006 Clinical comparison of head and neck and prostate IMRT plans using absorbed dose to medium and absorbed dose to water *Phys. Med. Biol.* **51** 4967-80

Dosanjh M, Jones B, Pawelke J, Pruschy M and Sørensen B S 2018 Overview of research and therapy facilities for radiobiological experimental work in particle therapy. Report from the European Particle Therapy Network radiobiology group *Radiother. Oncol.* **128** 14-8

du Plessis F C, Willemse C A, Lotter M G and Goedhals L 1998 The indirect use of CT numbers to establish material properties needed for Monte Carlo calculation of dose distributions in patients *Med. Phys.* **25** 1195-201

España S and Paganetti H 2010 The impact of uncertainties in the CT conversion algorithm when predicting proton beam ranges in patients from dose and PET-activity distributions *Phys. Med. Biol.* **55** 7557

Eulitz J, Lutz B, Wohlfahrt P, Dutz A, Enghardt W, Karpowitz C, Krause M, Troost E G C and Lühr A 2019a A Monte Carlo based radiation response modelling framework to assess variability of clinical RBE in proton therapy *Phys. Med. Biol.* **64** 225020

Eulitz J, Troost E G C, Raschke F, Schulz E, Lutz B, Dutz A, Löck S, Wohlfahrt P, Enghardt W, Karpowitz C, Krause M and Lühr A 2019b Predicting late magnetic resonance image changes in glioma patients after proton therapy *Acta Oncol.* **58** 1536-9

Fippel M and Nüsslin F 2000 Comments on `Converting absorbed dose to medium to absorbed dose to water for Monte Carlo based photon beam dose calculations' *Phys. Med. Biol.* **45** L17-L8

Giebeler A, Newhauser W D, Amos R A, Mahajan A, Homann K and Howell R M 2013 Standardized treatment planning methodology for passively scattered proton craniospinal irradiation *Radiation Oncology* **8** 32

Grassberger C, Daartz J, Dowdell S, Ruggieri T, Sharp G and Paganetti H 2014 Quantification of Proton Dose Calculation Accuracy in the Lung *Int. J. Radiat. Oncol. Biol. Phys.* **89** 424-30

Guatelli S and Incerti S 2017 Monte Carlo simulations for medical physics: From fundamental physics to cancer treatment *Phys. Med.* **33** 179-81

Hünemohr N, Paganetti H, Greilich S, Jäkel O and Seco J 2014 Tissue decomposition from dual energy CT data for MC based dose calculation in particle therapy *Med. Phys.* **41** 061714

Jiang H, Seco J and Paganetti H 2007 Effects of Hounsfield number conversion on CT based proton Monte Carlo dose calculations *Med. Phys.* **34** 1439-49

Lalonde A and Bouchard H 2016 A general method to derive tissue parameters for Monte Carlo dose calculation with multi-energy CT *Phys. Med. Biol.* **61** 8044-69

Lalonde A, Xie Y, Burgdorf B, O'Reilly S, Ingram W S, Yin L, Zou W, Dong L, Bouchard H and Teo B-K K 2019 Influence of intravenous contrast agent on dose calculation in proton therapy using dual energy CT *Phys. Med. Biol.* **64** 125024

Landry G, Parodi K, Wildberger J E and Verhaegen F 2013 Deriving concentrations of oxygen and carbon in human tissues using single- and dual-energy CT for ion therapy applications *Phys. Med. Biol.* **58** 5029-48

Möhler C, Wohlfahrt P, Richter C and Greilich S 2016 Range prediction for tissue mixtures based on dual-energy CT *Phys. Med. Biol.* **61** N268

Paganetti H 2009 Dose to water versus dose to medium in proton beam therapy *Phys. Med. Biol.* **54** 4399

Paganetti H 2012 Range uncertainties in proton therapy and the role of Monte Carlo simulations *Phys. Med. Biol.* **57** R99-R117

Paganetti H, Jiang H, Parodi K, Slopsema R and Engelsman M 2008 Clinical implementation of full Monte Carlo dose calculation in proton beam therapy *Phys. Med. Biol.* **53** 4825

Perl J 2016 User Guide for TOPAS Version 3.0.

Perl J, Shin J, Schuemann J, Faddegon B and Paganetti H 2012 TOPAS: an innovative proton Monte Carlo platform for research and clinical applications *Med. Phys.* **39** 6818-37

Schneider U, Pedroni E and Lomax A 1996 The calibration of CT Hounsfield units for radiotherapy treatment planning *Phys. Med. Biol.* **41** 111-24

Schneider W, Bortfeld T and Schlegel W 2000 Correlation between CT numbers and tissue parameters needed for Monte Carlo simulations of clinical dose distributions *Phys. Med. Biol.* **45** 459

Siebers J V, Keall P J, Nahum A E and Mohan R 2000 Converting absorbed dose to medium to absorbed dose to water for Monte Carlo based photon beam dose calculations *Phys. Med. Biol.* **45** 983-95

Taasti V T, Bäumer C, Dahlgren C V, Deisher A J, Ellerbrock M, Free J, Gora J, Kozera A, Lomax A J, De Marzi L, Molinelli S, Kevin Teo B-K, Wohlfahrt P, Petersen J B B, Muren L P, Hansen D C and Richter C 2018 Inter-centre variability of CT-based stopping-power prediction in particle therapy: Survey-based evaluation *Physics and Imaging in Radiation Oncology* **6** 25-30

Vanderstraeten B, Chin P W, Fix M, Leal A, Mora G, Reynaert N, Seco J, Soukup M, Spezi E, De Neve W and Thierens H 2007 Conversion of CT numbers into tissue parameters for Monte Carlo dose calculations: a multi-centre study *Phys. Med. Biol.* **52** 539-62

White D R, Booz J, Griffith R V, Spokas J J and Wilson I J 1989 ICRU Report 44: Tissue Substitutes in Radiation Dosimetry and Measurement *International Commission on Radiation Units and Measurements*

Wohlfahrt P, Möhler C, Hietschold V, Menkel S, Greilich S, Krause M, Baumann M, Enghardt W and Richter C 2017a Clinical Implementation of Dual-energy CT for Proton Treatment Planning on Pseudo-monoenergetic CT scans *Int. J. Radiat. Oncol. Biol. Phys.* **97** 427-34

Wohlfahrt P, Möhler C, Richter C and Greilich S 2018a Evaluation of Stopping-Power Prediction by Dual- and Single-Energy Computed Tomography in an Anthropomorphic Ground-Truth Phantom *Int. J. Radiat. Oncol. Biol. Phys.* **100** 244-53

Wohlfahrt P, Möhler C, Stützer K, Greilich S and Richter C 2017b Dual-energy CT based proton range prediction in head and pelvic tumor patients *Radiother. Oncol.* **125** 526-33

Wohlfahrt P, Möhler C, Troost E G C, Greilich S and Richter C 2019 Dual-Energy Computed Tomography to Assess Intra- and Inter-Patient Tissue Variability for Proton Treatment Planning of Patients With Brain Tumor *Int. J. Radiat. Oncol. Biol. Phys.*

Wohlfahrt P and Richter C 2020 Status and innovations in pre-treatment CT imaging for proton therapy *The British Journal of Radiology* **93** 20190590

Wohlfahrt P, Troost E G C, Hofmann C, Richter C and Jakobi A 2018b Clinical Feasibility of Single-Source Dual-spiral 4D Dual-Energy CT for Proton Treatment Planning Within the Thoracic Region *Int. J. Radiat. Oncol. Biol. Phys.* **102** 830-40

Woodard H Q and White D R 1986 The composition of body tissues *Br. J. Radiol.* **59** 1209-18

Wu S W, Tung C J, Lee C C, Fan K H, Huang H C and Chao T C 2015 Impact of the material composition on proton range variation – A Monte Carlo study *RaPC* **116** 199-202

Zhang R and Newhauser W D 2009 Calculation of water equivalent thickness of materials of arbitrary density, elemental composition and thickness in proton beam irradiation *Phys. Med. Biol.* **54** 1383-95

Zhang R, Taddei P J, Fitzek M M and Newhauser W D 2010 Water equivalent thickness values of materials used in beams of protons, helium, carbon and iron ions *Phys. Med. Biol.* **55** 2481-93